

Quantum superposition of distinct macroscopic states

Jonathan R. Friedman, Vijay Patel, W. Chen, S. K. Tolpygo & J. E. Lukens

Department of Physics and Astronomy, The State University of New York, Stony Brook, New York 11794-3800, USA

In 1935, Schrödinger¹ attempted to demonstrate the limitations of quantum mechanics using a thought experiment in which a cat is put in a quantum superposition of alive and dead states. The idea remained an academic curiosity until the 1980s when it was proposed²⁻⁴ that, under suitable conditions, a macroscopic object with many microscopic degrees of freedom could behave quantum mechanically, provided that it was sufficiently decoupled from its environment. Although much progress has been made in demonstrating the macroscopic quantum behaviour of various systems such as superconductors⁵⁻⁹, nanoscale magnets¹⁰⁻¹², laser-cooled trapped ions¹³, photons in a microwave cavity¹⁴ and C₆₀ molecules¹⁵, there has been no experimental demonstration of a quantum superposition of truly macroscopically distinct states. Here we present experimental evidence that a superconducting quantum interference device (SQUID) can be put into a superposition of two magnetic-flux states: one corresponding to a few microamperes of current flowing clockwise, the other corresponding to the same amount of current flowing anticlockwise.

The simplest SQUID (the radio frequency (r.f.) SQUID) is a superconducting loop of inductance L broken by a Josephson tunnel junction with capacitance C and critical current I_c . In equilibrium, a dissipationless supercurrent can flow around this loop, driven by the difference between the flux Φ that threads the loops and the external flux Φ_x applied to the loop. The dynamics of the SQUID can be described in terms of the variable Φ and are analogous to those of a particle of 'mass' C (and kinetic energy $\frac{1}{2}C\dot{\Phi}^2$) moving in a one-dimensional potential (Fig. 1a) given by the sum of the magnetic energy of the loop and the Josephson coupling energy of the junction:

$$U = U_0 \left[\frac{1}{2} \left(\frac{2\pi(\Phi - \Phi_x)}{\Phi_0} \right)^2 - \beta_L \cos(2\pi\Phi/\Phi_0) \right] \quad (1)$$

where Φ_0 is the flux quantum, $U_0 \equiv \Phi_0^2/4\pi^2L$ and $\beta_L \equiv 2\pi LI_c/\Phi_0$. For the parameters used in our experiment, this a double-well potential separated by a barrier with a height depending on I_c . When $\Phi_x = \Phi_0/2$ the potential is symmetric. Any change in Φ_x then tilts the potential, as shown in Fig. 1a.

As required by quantum mechanics, in the dissipationless state the phase of the macroscopic superconducting wavefunction must vary continuously around the loop, increasing by an integer f times 2π when one winds once around the loop. The quantum number f defines the 'fluxoid' state of the SQUID. In Fig. 1a, the left (right) well corresponds to $f = 0$ (1) in which a static current ($>1 \mu\text{A}$ for our system) flows around the loop in such a way as to tend to cancel (augment) Φ_x . Classically, a transition between the $f = 0$ and $f = 1$ wells involves passage over the top of the barrier. Quantum mechanically, however, the system can tunnel through the barrier. For weak damping, the system has quantized energy levels that, considerably below the barrier, are localized in each well. At various values of Φ_x , levels in opposite wells will align, giving rise to resonant tunnelling between the wells⁵. During this interwell transition Φ changes by some fraction of Φ_0 , or—stated in different terms—the magnetic moment of the system changes by a macroscopic amount, in this case by over $10^{10} \mu_B$. Until now, however, there has been no evidence that the tunnelling process between these macroscopically distinct states could be coherent, that is, that the

SQUID could be put into a coherent superposition of two flux states in different wells.

Such a superposition would manifest itself in an anticrossing, as illustrated in Fig. 1b, where the energy-level diagram of two levels of different fluxoid states (labelled $|0\rangle$ and $|1\rangle$) is shown in the neighbourhood in which they would become degenerate without coherent interaction (dashed lines). Coherent tunnelling lifts the degeneracy (solid lines) so that at the degeneracy point the energy eigenstates are $1/\sqrt{2}(|0\rangle + |1\rangle)$ and $1/\sqrt{2}(|0\rangle - |1\rangle)$, the symmetric and anti-symmetric superpositions. The energy difference ΔE between the two states is given approximately by $\Delta E = \sqrt{\epsilon^2 + \Delta^2}$, where Δ is known as the tunnel splitting. The goal of the present work is to demonstrate the existence of such a splitting and, thereby the coherent superposition of macroscopically distinct flux states.

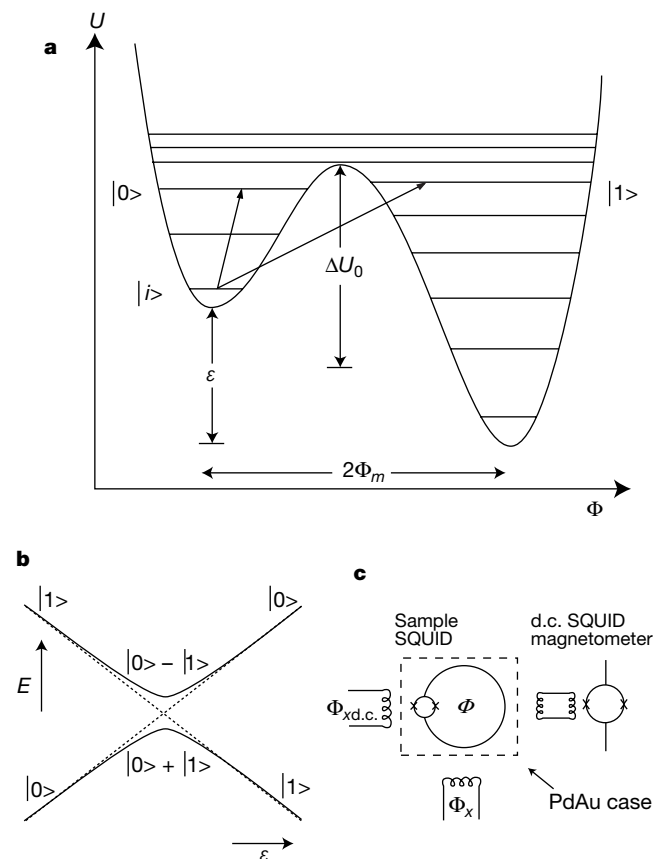


Figure 1 SQUID potential, energy-level anticrossing and experimental set-up. **a**, SQUID potential. The left well corresponds to the zero-fluxoid state and the right well to the one-fluxoid state. Energy levels are localized in each well. Both the tilt ϵ and energy barrier at zero tilt ΔU_0 can be varied *in situ* in the experiments. The process of photon-induced interwell transitions is illustrated by the arrows, where the system is excited out of the initial state $|i\rangle$ and into one of two excited states $|0\rangle$ or $|1\rangle$. **b**, Schematic anticrossing. When the two states $|0\rangle$ and $|1\rangle$ would become degenerate in the absence of coherence, the degeneracy is lifted and the states of the system are the symmetric and antisymmetric superpositions of the flux-basis states: $1/\sqrt{2}(|0\rangle + |1\rangle)$ and $1/\sqrt{2}(|0\rangle - |1\rangle)$. **c**, Experimental set-up. Our SQUID contains a 'tunable junction', a small d.c.-SQUID. A flux $\Phi_{\text{d.c.}}$ applied to this small loop tunes the barrier height ΔU_0 . Another flux Φ_x tunes the tilt ϵ of the potential. A separate d.c.-SQUID acts as a magnetometer, measuring the flux state of the sample. The sample SQUID used in our experiments is characterized by the following three energies: the charging energy $E_c \equiv e^2/2C = 9.0$ mK, the inductive energy $E_L \equiv \Phi_0^2/2L = 645$ K and a tunable Josephson coupling energy $E_J = (I_c \Phi_0/2\pi) \cos(\pi \Phi_{\text{d.c.}}/\Phi_0) = 76 \text{ K} \cos(\pi \Phi_{\text{d.c.}}/\Phi_0)$. The plasma frequency ω_J (the frequency of small oscillations in the bottom of a well) associated with these parameters is $1.5\text{--}1.8 \times 10^{11} \text{ rad s}^{-1}$, depending on the value of $\Phi_{\text{d.c.}}$. The fact that $E_c \ll E_L, E_J$ confirms that flux is the proper basis to describe the SQUID's dynamics.

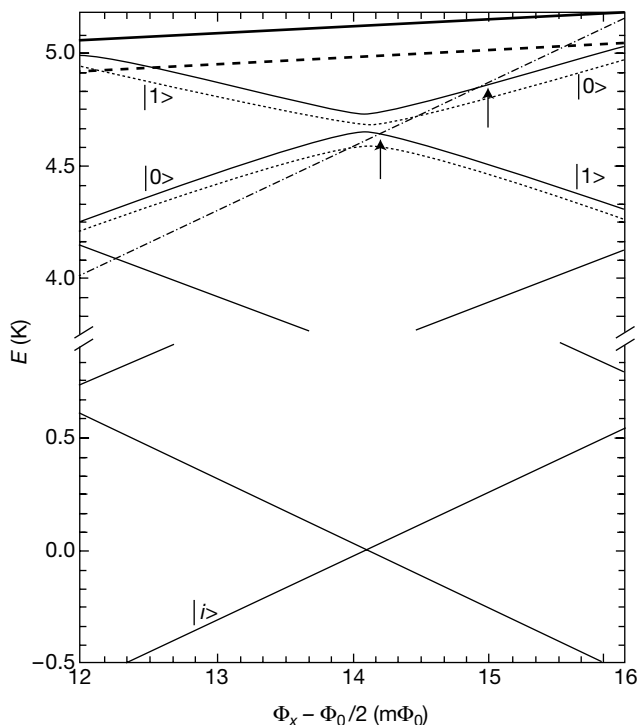


Figure 2 Calculated energy levels and photon-assisted tunnelling process. The thin solid lines represent the calculated SQUID energy levels as a function of Φ_x for a barrier height of $\Delta U_0 = 9.117$ K. The thick solid line is the calculated top of the energy barrier. The 96.0 GHz (4.61 K) applied microwaves boost the system out of the initial state $|i\rangle$, bringing it almost to the dot-dashed line. At certain values for Φ_x for which this line intersects one of the excited states (indicated by the arrows), a photon is absorbed and the system has a large probability of making an interwell transition. When the ΔU_0 is reduced (to 8.956 K), the levels and top of the barrier move down relative to $|i\rangle$ (dotted lines), changing the values of Φ_x at which photon absorption occurs. All energies are calculated relative to the mean energy of $|i\rangle$ and the lowest state of the right well; for clarity, the zero of energy is shifted to the point where the levels in the lower part of the figure cross.

A necessary condition for resolving this splitting is that the experimental linewidth of the states be smaller than Δ (ref. 16). The SQUID is extremely sensitive to external noise and dissipation (including that due to the measurement of Φ), both of which broaden the linewidth. Thus, the experimental challenges to observing coherent tunnelling are severe. The measurement apparatus must be weakly coupled to the system to preserve coherence, while the signal strength must be sufficiently large to resolve the closely spaced levels. In addition, the system must be well shielded from external noise. These challenges have frustrated previous attempts^{5,6} to observe coherence in SQUIDs.

The SQUID used in these experiments is made up of two Nb/AlO_x/Nb tunnel junctions in parallel, as shown in Fig. 1c; this essentially acts as a tunable junction in which I_c can be adjusted with an applied flux $\Phi_{x,d.c.}$. Thus, with Φ_x we control the tilt ϵ of the potential in Fig. 1a, while with $\Phi_{x,d.c.}$ we control ΔU_0 , the height of the energy barrier at $\epsilon = 0$. The flux state of our sample is measured by a separate d.c.-SQUID magnetometer inductively coupled to the sample. The sample is encased in a PdAu shield that screens it from unwanted radiation; a coaxial cable entering the shield allows the application of controlled external microwaves. The set-up is carefully filtered and shielded, as described elsewhere^{5,6}, and cooled to about 40 mK in a dilution refrigerator.

In our experiments, we probe the anticrossing of two excited levels in the potential by using microwaves to produce photon-assisted tunnelling. Figure 1a depicts this process for the case where the levels $|0\rangle$ and $|1\rangle$ are each localized in opposite wells. The system is initially prepared in the lowest state in the left well (labelled $|i\rangle$) with the barrier high enough that the rate for tunnelling out of $|i\rangle$ is negligible on the timescale of the measurement. Microwave radiation is then applied. When the energy difference between the initial state and an excited state matches the radiation frequency, the system has an appreciable probability of being excited into this state and subsequently decaying into the right well. This transition between wells results in a change in flux that can be detected by the magnetometer. Figure 2 shows the photon-assisted process when the excited levels have an anticrossing. From the SQUID's parameters (see below) and potential (equation (1)), it is straightforward to numerically solve for the energy levels of the SQUID in the zero-damping (completely coherent) limit. In Fig. 2 calculated levels (for $\Delta U_0 = 9.117$ K) are plotted as a function of Φ_x (thin solid lines). The calculated top of the barrier is indicated by the thick solid

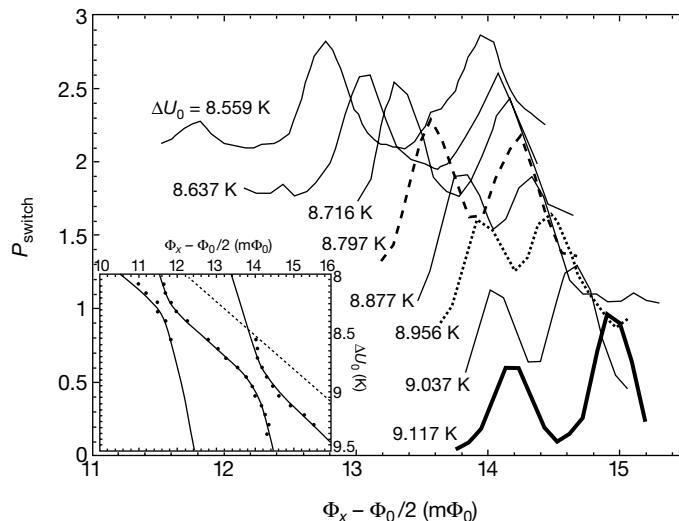


Figure 3 Experimental data. The main figure shows, as a function of Φ_x , the probability P_{switch} of making an interwell transition when a millisecond pulse of 96-GHz microwave radiation is applied. For clarity, each curve is shifted vertically by 0.3 relative to the previous one. As the energy barrier is reduced, the two observed peaks move closer

together and then separate: the signature of an anticrossing. The inset shows the position of the observed peaks in the $\Delta U_0 - \Phi_x$ plane. Also shown is the calculated locus of points at which the virtual photon level (dot-dashed line in Fig. 2) intersects an excited level (solid lines) or the top of the classical energy barrier (dashed line).

line. The dot-dashed line represents level $|i\rangle$ shifted upward by the energy of the microwaves. At values of Φ_x for which this line intersects one of the excited levels (indicated by the arrows), the system can absorb a photon and make an interwell transition. When the barrier is reduced (to $\Delta U_0 = 8.956$ K), the excited levels and top of the barrier move to lower energy relative to $|i\rangle$ (dotted lines in the figure) and photon absorption occurs at different values of Φ_x . For a fixed frequency (a fixed frequency is used to ensure that the microwave power coupled to the sample remains constant for all resonances), we can map out the anticrossing by progressively reducing the barrier and thus moving the levels through the dashed photon line.

We use pulsed microwaves to excite the system to the upper levels. Before each pulse, the system is prepared in state $|i\rangle$ and the values of ΔU_0 and ϵ are set. Millisecond pulses of 96-GHz microwave radiation at a fixed power are applied and the probability of making a transition is measured. The experiment is repeated for various values of ϵ and ΔU_0 . Data from these measurements are shown in Fig. 3, where the probability of making a photon-assisted interwell transition is plotted as a function of Φ_x . Each curve, for a given ΔU_0 , is shifted vertically for clarity. Two sets of peaks are clearly seen. As ΔU_0 is decreased, these peaks move closer together and then separate without crossing. For $\Delta U_0 = 9.117$ K (thick solid curve), the right peak roughly corresponds to level $|0\rangle$, which is localized in the same well as $|i\rangle$ (compare with Fig. 2). The relative amplitude of the two peaks is due to the asymmetry of the potential (for this data, $|0\rangle$ is the fourth excited level in the left well and $|1\rangle$ is the tenth excited level in the right well) and is in accordance with recent calculations¹⁶. When ΔU_0 is decreased to 8.956 K (dotted curve), the peaks move closer together and the asymmetry disappears. The two states are now in the coherent regime and correspond approximately to the symmetric and anti-symmetric superpositions of the $|0\rangle$ and $|1\rangle$ states. As the barrier is decreased further (8.797 K is the dashed curve), the peaks move apart again and the asymmetry reappears, but now with a larger left peak and corresponding to $|0\rangle$. The two levels have thus passed through the anticrossing, changing roles without actually intersecting. The inset shows the positions of the peaks in the main figure (as well as other peaks) in the ΔU_0 - Φ_x plane; two anticrossings are clearly seen. The solid (dashed) lines in the inset represent the locus of points when the calculated energy levels (top of the barrier) are 96 GHz above the state $|i\rangle$. All of our data lie to the left of the dashed line and, therefore, correspond to levels that are below the top of the barrier. Hence, the flux-basis

states $|0\rangle$ and $|1\rangle$ are macroscopically distinct with mean fluxes that, we calculate, differ by about $\frac{1}{4}\Phi_0$. Each observed anticrossing thus represents the coherent superposition of macroscopically distinct states.

For one of the anticrossings, Fig. 4 shows the energy of the levels $|0\rangle$ and $|1\rangle$ as a function of ϵ relative to their mean energy, $E_{\text{mean}}(\Delta U_0, \Phi_x)$, calculated for each experimental point using the parameters listed below. This makes the data manifestly similar to Fig. 1b. At the middle of the anticrossing, the two levels have a tunnel splitting Δ of about 0.1 K in energy while the upper level is still about 0.15 K below the top of the classical energy barrier.

There are three parameters used for the calculations presented in Figs 3 and 4; $L, Z \equiv \sqrt{L/C}$ and β_L , all of which can be independently determined from measurements of classical phenomena or incoherent resonant tunnelling in the absence of radiation. From these independent measurements, we find $L = 240 \pm 15$ pH, $Z = 48.0 \pm 0.1 \Omega$ and $\beta_L = 2.33 \pm 0.01$. The values used in the calculation that yielded the best agreement with the data are $L = 238$ pH, $Z = 48 \Omega$ and $\beta_L = 2.35$, all in good agreement with the independently determined values.

We stress two related points regarding these results. First, at the anticrossing, both levels are below the top of the classical energy barrier. This is essential for the system to be in a superposition of macroscopically distinct flux states since the levels (in the absence of coherence) can only be associated with one well (one fluxoid state) if they are below the top of the barrier. The second point concerns the meaning of ‘macroscopic’. The SQUID exhibits macroscopic quantum behaviour in two senses: (1) The quantum dynamics of the SQUID is determined by the flux through the loop, a collective coordinate representing the motion of approximately 10^9 Cooper pairs acting in tandem. Since the experimental temperature is about 500 times smaller than the superconducting energy gap, almost all microscopic degrees of freedom are frozen out and only the collective flux coordinate retains any dynamical relevance. (2) The two flux-basis states that we find to be superposed are macroscopically distinct. We calculate that for the anticrossings measured, the states $|0\rangle$ and $|1\rangle$ differ in flux by more than $\frac{1}{4}\Phi_0$ and differ in current by $2\text{--}3 \mu\text{A}$. Given the geometry of the SQUID, this corresponds to a local magnetic moment of about $10^{10} \mu_B$, a truly macroscopic moment. □

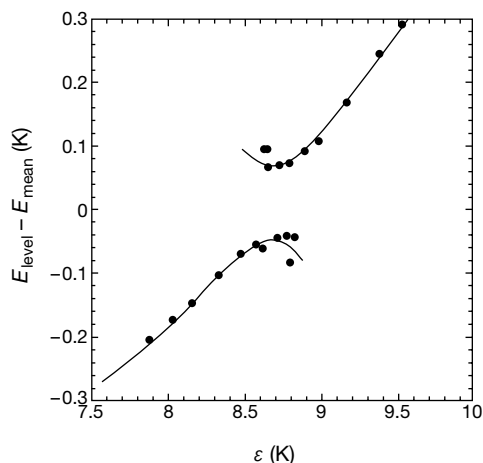


Figure 4 Energy of the measured peaks relative to the calculated mean of the two levels as a function of ϵ . At the midpoint of the figure, the measured tunnel splitting Δ between the two states in this anticrossing is about 0.1 K and the upper level is about 0.15 K below the top of the classical energy barrier. Calculated energy levels are indicated by the lines.

Received 12 April; accepted 8 June 2000.

- Schrödinger, E. Die gegenwärtige situation in der quantenmechanik. *Naturwissenschaften* **23**, 807–812, 823–828, 844–849 (1935).
- Caldeira, A. O. & Leggett, A. J. Influence of dissipation on quantum tunneling in macroscopic systems. *Phys. Rev. Lett.* **46**, 211–214 (1981).
- Leggett, A. J. *et al.* Dynamics of the dissipative 2-state system. *Rev. Mod. Phys.* **59**, 1–85 (1987).
- Weiss, U., Grabert, H. & Linkwitz, S. Influence of friction and temperature on coherent quantum tunneling. *J. Low Temp. Phys.* **68**, 213–244 (1987).
- Rouse, R., Han, S. & Lukens, J. E. Observation of resonant tunneling between macroscopically distinct quantum levels. *Phys. Rev. Lett.* **75**, 1614–1617 (1995).
- Rouse, R., Han, S. & Lukens, J. E. in *Phenomenology of Unification from Present to Future* (eds Palazzi, G. D., Cosmelli, C. & Zanello, L.) 207–224 (World Scientific, Singapore, 1998).
- Clarke, J., Cleland, A. N., Devoret, M. H., Esteve, D. & Martinis, J. M. Quantum mechanics of a macroscopic variable: the phase difference of a Josephson junction. *Science* **239**, 992–997 (1988).
- Silvestrini, P., Palmieri, V. G., Ruggiero, B. & Russo, M. Observation of energy level quantization in underdamped Josephson junctions above the classical-quantum regime crossover temperature. *Phys. Rev. Lett.* **79**, 3046–3049 (1997).
- Nakamura, Y., Pashkin, Y. A. & Tsai, J. S. Coherent control of macroscopic quantum states in a single-Cooper-pair box. *Nature* **398**, 786–788 (1999).
- Friedman, J. R., Sarachik, M. P., Tejada, J. & Ziolo, R. Macroscopic measurement of resonant magnetization tunneling in high-spin molecules. *Phys. Rev. Lett.* **76**, 3830–3833 (1996).
- del Barco, E. *et al.* Quantum coherence in Fe_8 molecular nanomagnets. *Europhys. Lett.* **47**, 722–728 (1999).
- Wernsdorfer, W. *et al.* Macroscopic quantum tunneling of magnetization of single ferrimagnetic nanoparticles of barium ferrite. *Phys. Rev. Lett.* **79**, 4014–4017 (1997).
- Monroe, C., Meekhof, D. M., King, B. E. & Wineland, D. J. A “Schrödinger cat” superposition state of an atom. *Science* **272**, 1131–1136 (1996).
- Brune, M. *et al.* Observing the progressive decoherence of the “meter” in a quantum measurement. *Phys. Rev. Lett.* **77**, 4887–4890 (1996).
- Arndt, M. *et al.* Wave–particle duality of C_{60} molecules. *Nature* **401**, 680–682 (1999).
- Averin, D., Friedman, J. R. & Lukens, J. E. Macroscopic resonant tunneling of magnetic flux. Preprint cond-mat/0005081 at xxx.lanl.gov (2000).

Acknowledgements

We thank D. Averin and S. Han for useful conversations, J. Männik, R. Rouse and A. Lipski for technical advice and assistance and M. P. Sarachik for the loan of some equipment. This work was supported by the US Army Research Office and the US National Science Foundation.

Correspondence and requests for materials should be addressed to J.R.F. (e-mail: jonathan.friedman@sunysb.edu).

Generation and detection of phase-coherent current-driven magnons in magnetic multilayers

M. Tsoi*, A. G. M. Jansen*, J. Bass†, W.-C. Chiang†, V. Tsoi‡ & P. Wyder*

* Grenoble High Magnetic Field Laboratory, Max-Planck-Institut für Festkörperforschung and Centre National de la Recherche Scientifique, BP 166, F-38042 Grenoble Cedex 9, France

† Department of Physics and Astronomy, Michigan State University, East Lansing, Michigan 48824-1116, USA

‡ Institute of Solid State Physics RAS, 142432 Chernogolovka, Moscow Region, Russia

The magnetic state of a ferromagnet can affect the electrical transport properties of the material; for example, the relative orientation of the magnetic moments in magnetic multilayers¹ underlies the phenomenon of giant magnetoresistance. The inverse effect—in which a large electrical current density can perturb the magnetic state of a multilayer—has been predicted^{2–7} and observed experimentally with point contacts^{8,9} and lithographically patterned samples^{10,11}. Some of these observations were taken as indirect evidence for current-induced excitation of spin waves, or ‘magnons’. Here we probe directly the high-frequency behaviour and partial phase coherence of such current-induced excitations, by externally irradiating a point contact with microwaves. We determine the magnon spectrum and investigate how the magnon frequency and amplitude vary with the exciting current. Our observations support the feasibility of a spin-wave maser² or ‘SWASER’ (spin-wave amplification by stimulated emission of radiation).

A spin-momentum transfer associated with an electric current traversing a magnetic multilayer has been predicted^{2–7} to stimulate the emission of spin waves if the current density is large enough. In our experiments we inject current densities as high as 10^8 A cm^{-2} into a multilayer through a point contact made by bringing a sharpened silver tip into contact with the multilayer film^{12,13}. Such a geometry, where a laterally unbounded multilayer is excited by a d.c. current whose distribution is localized by means of a point contact was shown⁷ to be equivalent to the case of a bounded multilayer^{2–3} of diameter comparable to that of the point contact. In both cases, spin-polarized currents induce a torque on magnetic moments in the ferromagnetic layers, thereby exciting their precession (spin waves). However, in the bounded multilayer this torque is applied to an entire magnetic layer, but in our case it is applied only to a small region of the layer just under the contact (the ‘disk’, for a circular contact), where the density of applied current is large enough. Spin-wave excitation is therefore expected only in this disk under the contact⁷. We⁸ and others⁹ have observed step increases in the static resistance ($R = V/I$) of such contacts for a certain bias current (see, for instance, equivalent peak structures in the derivative contact resistance dV/dI in Fig. 1b), attributable to the onset of magnon generation in the multilayer. Nevertheless, the main issue—the high-frequency nature of the excitation—was not conclusively addressed as magnetization reversal alone results in a similar increase in resistance^{9,11}.

To probe the frequencies of the current-driven magnons we have placed the point contact inside the microwave cavity of an electron spin resonance (ESR) spectrometer¹⁴, as shown schematically in Fig. 1a. Injection via a point contact of a high current density into the multilayer induces high-frequency precession of magnetization in the disk at frequency ω_1 . Using the ESR spectrometer to apply external radio-frequency radiation at frequency ω_2 , we expect to see a resonant amplification of this current-induced precession when ω_2 equals ω_1 . This process leads to an additional d.c. voltage across the contact that allows the frequency of precession to be mapped for different applied currents and fields. Here the contact serves as a lumped circuit element (much as rectifiers¹⁵ and frequency mixing diodes¹⁶ are used in radio engineering) that mixes the high-frequency response of the injected current (for example, radiation by current-driven magnons) with the external microwave radiation. The electromagnetic radiation couples into the contact junction through the wire tip, which acts as an antenna, thereby inducing high-frequency currents in the junction. For a point contact irradiated with an electromagnetic field that has components at two frequencies ω_1 and ω_2 , the junction current is

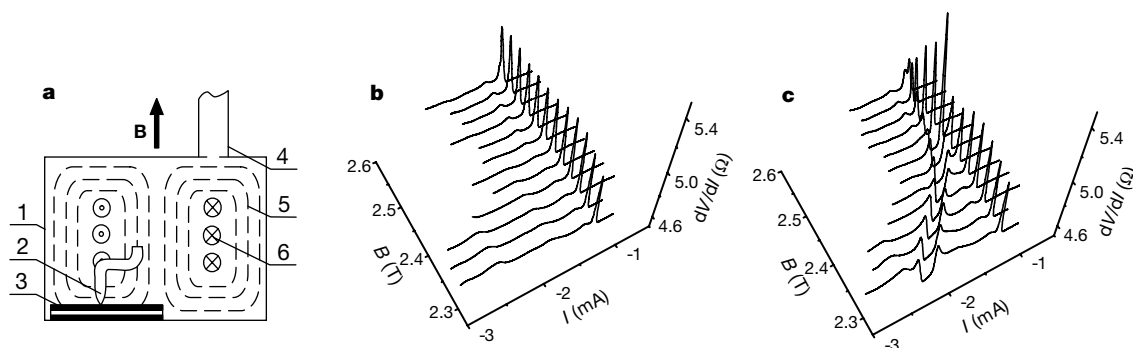


Figure 1 Experimental geometry and typical influence of the externally applied radiation on point-contact characteristics. **a**, Diagram of experimental geometry: 1, microwave cavity; 2, silver tip; 3, multilayer sample; 4, waveguide; 5 and 6 indicate magnetic and electric microwave field pattern. **b, c**, The point contact dV/dI spectra (solid lines) for a series of magnetic fields without (**b**) and with (**c**) external irradiation of the point contact with microwaves at $\omega/2\pi = 50.6 \text{ GHz}$. Without irradiation (**b**) the spectra reveal just the usual peak structure for a certain negative bias current $I^*(B) \approx -1.2 \text{ mA}$ that we attribute

to the onset of the current-driven magnon excitations. Irradiation of the contact with microwaves (**c**) generates an additional structure in dV/dI . The strongest influence of the microwaves is found around a certain value $B^* \approx 2.6 \text{ T}$ of the applied field. Starting down from high fields, the additional structure is absent above B^* , appears around I^* when the field approaches B^* , and then moves to higher values of the bias current I as the field is reduced below B^* .